Available online at www.sciencedirect.com
ScienceDirect
European Journal of Mechanics B/Fluids 26 (2007) 615–631

A comparison between different asymmetric abdominal aortic aneurysm morphologies employing computational fluid–structure interaction analysis

Zhonghua Li [a], Clement Kleinstreuer [b,*]

[a] *Endovascular Division of Cordis Corporation, a Johnson & Johnson Company, Warren, NJ 07059, USA*
[b] *Department of Mechanical and Aerospace Engineering and Department of Biomedical Engineering, North Carolina State University, Raleigh, NC 27695-7910, USA*

Received 20 April 2005; received in revised form 1 December 2006; accepted 20 March 2007

Available online 4 April 2007

Abstract

Considering representative asymmetric aneurysms in the abdominal aorta, the transient 3-D blood flow and pressure distributions as well as aneurysm wall stresses were numerically analyzed. To obtain more realistic and accurate results for blood flow fields and wall stress distributions, a coupled fluid-flow and solid–structure solver was employed. Geometric abdominal aortic aneurysm (AAA) variations studied included the degree of asymmetry, neck angle and bifurcation angle, and hence their impacts on the hemodynamics and biomechanics. The simulation results indicated that the assumption of *symmetric* AAA geometry may underestimate AAA-wall stress considerably. The neck angle influences the blood flow field substantially. A large neck angle, resulting in strong wall curvatures near the proximal neck, can produce aggravating blood flow patterns and elevated wall stresses (Von Mises). The iliac bifurcation angle affects blood flow patterns insignificantly but plays an important role in wall-stress concentrations. The wall stress of lateral asymmetric AAAs is higher than for the anterior-posterior asymmetric types. The maximum wall stress-site is located near the anterior distal side for the anterior-posterior asymmetric AAA and the distal side towards the asymmetric bulge in the lateral asymmetric AAA.

Keywords: Pulsatile 3-D blood flow; Abdominal aortic aneurysms; AAA morphologies; Maximum wall stress

1. Introduction

An aneurysm is a focal dilation of a blood vessel to greater than 50% of its normal diameter. Aneurysms are most commonly found in the abdominal aorta where major complications may develop without definite warnings. The mortality rate of ruptured abdominal aortic aneurysms (AAAs) is up to 75%, making it the 13th leading cause of death in the US. Traditionally, a maximum-diameter-criterion of 5.5 cm has been employed for abdominal aortic aneurysms (AAAs) to indicate the need for surgical intervention in order to prevent rupture [1,2]. However, it is

* Corresponding author. Tel.: +1 919 515 5261; fax: +1 919 515 7968.
E-mail address: ck@eos.ncsu.edu (C. Kleinstreuer).
URL: http://www.mae.ncsu.edu/research/ck_CFPDlab/index.html.

0997-7546/$ – see front matter
doi:10.1016/j.euromechflu.2007.03.003

the actual maximum focal AAA-wall stress exceeding locally the AAA's yield stress which causes rupture [2]. So far, most *computational* research papers considered blood flow and wall stress analyses *separately*, employing the geometries of laboratory and clinical AAA models. For example, Yamada et al. [3] analyzed mechanical aspects of AAA growth and AAA rupture. They concluded that the diameter, wall thickness, and blood pressure play significant roles in AAA rupture. Employing finite element analysis, Raghavan et al. [4] simulated 3-D reconstructed AAA models and found that the 5-cm AAA-diameter criterion as a rupture predictor was not sufficient. Thubrikar et al. [5] studied the mechanical properties of the AAA wall and found that different regions of an AAA had different yield stresses, yield strains and other mechanical properties. They also found that the rupture of an AAA is most likely to occur on the inner surface of the wall. Fillinger et al. [1,2] performed in vivo as well as numerical analyses of mechanical wall stress and AAA-rupture risk based on realistic three-dimensional CT-scan AAA models. Vorp et al. [6] indicated that, in addition to diameter, the influence of asymmetry on mechanical wall stress in AAAs is very important. Finol et al. [7,8] investigated pulsatile flow in realistic asymmetric AAAs, employing numerical analyses. In terms of *experimental* investigations, Peattie et al. [9] used color Doppler flow imaging and laser Doppler velocimetry for steady and transient flow in AAA models and found that the increased turbulence might contribute significantly to the risk of rupture. Yip and Yu [10] measured with LDA the cyclic transition to turbulence in a rigid AAA model and indicated that the cyclic transition to turbulence may be vital to a better understanding of AAA growth and rupture. Yu [11] measured experimentally the steady and pulsatile flow patterns in a rigid abdominal aortic aneurysm model using an Particle Imaging device.

Because blood flow and vessel wall are coupled in a complicated way, the flow will affect movement of the walls and wall movements in turn influence the flow field to varying degrees. Thus, realistic and accurate analyses of the two-way interactions of pulsatile blood flow with the AAA wall, and hence the knowledge of pressure load, magnitude and location of the maximum wall stress, as well as the degree of wall distensiblility, are important in studying the hemodynamics and biomechanics of AAAs. However, most researchers simply consider structure and fluid flow separately, with the exception of a couple of research publications [12–14], which only performed simple AAA models without systemic flow studies. Thus, computer simulations of transient 3-D fluid–structure interactions for realistic AAAs can help to gain physical insight and make recommendations based on quantitative results. A coupled fluid-flow and solid–structure solver was employed to obtain more realistic and accurate hemodynamics and biomechanics results for AAAs. Specifically, three representative AAA configurations were considered for a typical cardiac input, in order to analyze blood flow fields and to evaluate critical AAA-wall parameter values.

2. Numerical method

2.1. System model and parameters

The governing equations for fluid flow and structure dynamics were discussed in our previous publications [15,16]. Although actual AAA configurations differ among patients, the three geometric parameters of interest are the aneurysm asymmetry, $\beta = l_1/l_2$ [6], the neck angle, θ, and the iliac bifurcation angle, φ (see Fig. 1(a)). Assuming laminar pulsatile blood flow in these AAAs with smooth elastic walls of variable thickness, the simulation of the fluid–structure interaction (FSI) dynamics requires the solution of two coupled sets of differential equations subject to measured inlet/outlet and no-slip surface conditions.

Blood is non-Newtonian, especially for strain rates $\dot{\gamma} < 200\ \mathrm{s}^{-1}$, the relationship between shear stress and rate-of-strain is nonlinear. The Quemada model is most suitable to describe the actual blood rheology, i.e., when the strain rate is $\geqslant 200\ \mathrm{s}^{-1}$ the equation automatically changes to Newtonian fluid flow behavior [17,18]. For our CT-scan based AAA models (Database: Patient Evaluation & Management Services, PEMS, West Lebanon, NH) within the physiologic range, the iliac bifurcation angle, neck angle and asymmetry index were statistically 56° (±23.7), 31.6° (±4.8) and 0.6 ± 0.2, respectively (see Table 1). Thus, typical iliac bifurcation angles of 55°, 90°, 120° and neck angle of 12°, 25° and 45° were selected.

Table 2 lists the structure parameter values used in the simulations. For the present range of blood pressure loads, i.e., 80–120 mmHg, linearly elastic, isotropic, homogeneous material properties were assumed to assess the AAA wall stress [6,12,19–22]. With respect to Young's moduli for the healthy arterial wall and aneurysm, experimental data indicate that Young's modulus of an aneurysm is much higher than for a healthy artery. In this paper, the aneurismal Young modulus is assumed to be 4.66 MPa [19]. The healthy artery (neck and iliac arteries) is incompressible with a

Table 1
CT-scan based AAA models

Patient number	306
Patient age (year)	74 ± 8.0
Follow-up duration (month)	9.0 ± 4.5
Maximum AAA diameter (mm)	53.7 ± 12.8
AAA volume (cm^3)	158 ± 90.6
Neck diameter (mm)	24.9 ± 3.8
Iliac diameter (mm)	13.6 ± 1.7
Iliac bifurcation angle (°)	56 ± 23.7
Neck angle (°)	31.6 ± 4.8
Asymmetry index	0.6 ± 0.2

Note: Values given as mean ± SD.

Table 2
Selected simulation parameters

Parameters	Neck aorta [19,6]	Iliac artery [24]	Aneurysm main-body [19,12,25]
Wall thickness	1.5 mm	1.0 mm	1.0–1.5 mm
Diameter	20 mm	12 mm	Maximum: 60 mm
Length	25 mm	35 mm	80 mm
Young's modulus	1.2 MPa	1.2 MPa	4.66 MPa
Poisson ratio	0.49	0.49	0.45
Density	1.121 g/cm^3	1.121 g/cm^3	1.121 g/cm^3

Poisson ratio of 0.49 [23], and the aneurysm wall is nearly incompressible with a Poisson ratio of 0.45 [12]. Based on the work of Thubrikar et al. [19], the wall thickness decreases gradually from the healthy neck to the maximum AAA diameter. In this paper, the wall thickness variation was based on the constant wall-volume assumption, i.e., the larger the diameter, the thinner is the wall thickness.

Flow boundary conditions included inlet velocity waveform and outlet pressure waveform based on measurements of a normal subject [26]. The physiologically representative inflow velocity waveform is shown in Fig. 1(b) with a maximum Reynolds number ($Re_{\max}$) of 1950 and average Reynolds number (Re_{average}) of 350. For the outlet pressure (see Fig. 1(b)(ii)), the peak and averaged pressures are 122 mmHg and 98.7 mmHg, respectively [26]. The pulse period was chosen to be $T = 1.2$ s. The inlet velocity profile is assumed to be parabolic. On the structure side, the boundary conditions included no temporal displacements at the inlet and the exit, and free displacement of the wall.

2.2. Numerical algorithm

The interactions between blood flow domain and blood vessel wall are strongly coupled, i.e., the flow will affect to various degrees movement of the walls and wall movements in turn influence the flow field. ANSYS (Ansys, Inc, 2003) is a suitable fluid–structure coupled solver which can deal with this FSI problem. The Arbitrary Lagrangian–Eulerian (ALE) formulation was set up in ANSYS to solve for the fluid–structure interactions. Specifically, in FSI problems, the fluid domain changes with time and the finite element mesh should move accordingly to satisfy the boundary conditions at the moving interfaces. ALE can determine the displacement at the beginning of each time step relative to the previous time step. For each time step, an elasticity-based morphing algorithm updates the mesh. The algorithm ensures that boundary layers are retained (i.e., nodes in a fine mesh area move less than nodes in a coarse mesh area). For large fluid domain changes, re-meshing is required. The governing equations for the fluid and solid domains are solved independently of each other. It transfers fluid forces, solid displacements, and velocities across the fluid–solid interface. The algorithm continues to loop through the solid and fluid analyses until convergence is reached for each time step. Convergence in the stagger loop is based on the quantities being transferred at the fluid–solid interface. Fig. 2 shows the algorithm for the time and stagger loops of the fluid–structure interaction analysis.

Even though linearly elastic material properties were assumed [6,12], the complex geometry of AAA exhibits strong geometric nonlinear behavior, i.e., the geometric nonlinear (large deformation) algorithm was employed to obtain more accurate results [19,27]. Hence, for the present simulations, analysis schemes accommodating geometric

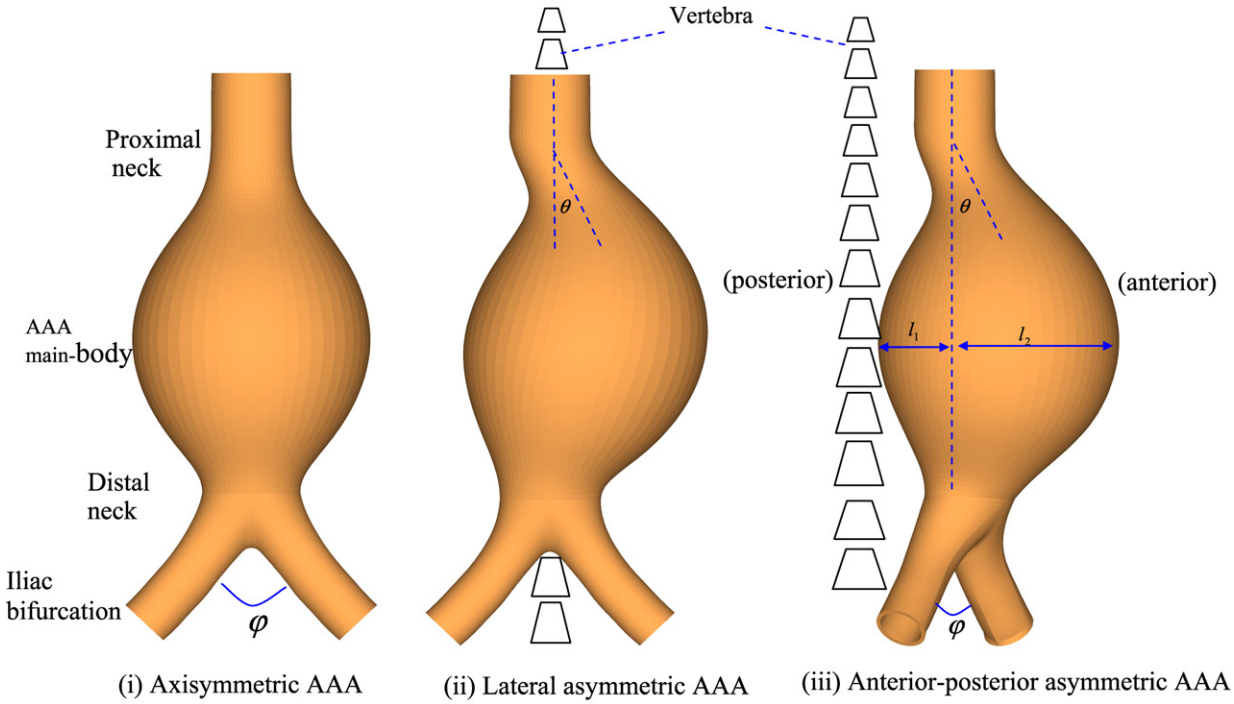

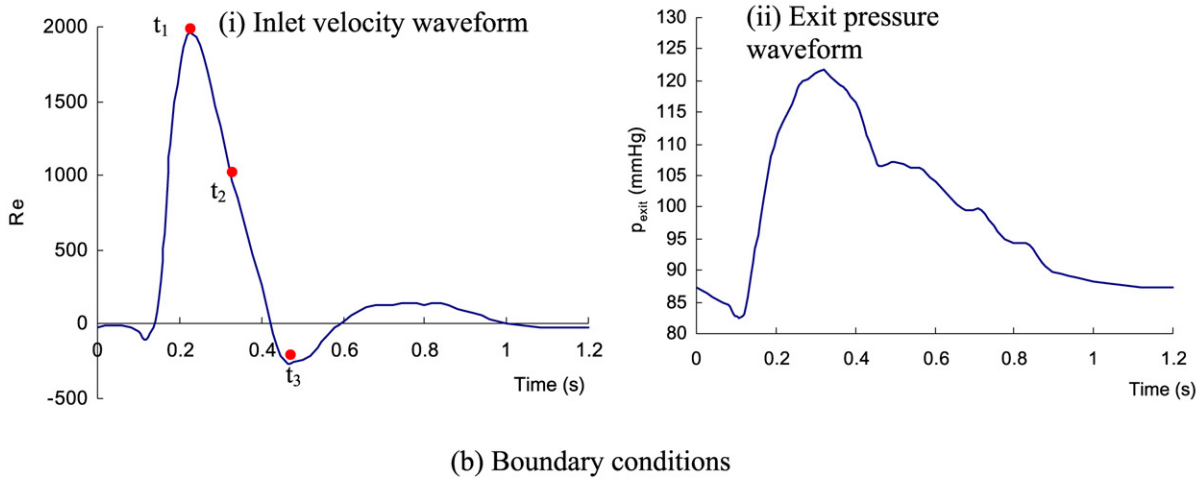

Fig. 1. (a) Schematic of AAA models. (b) Inlet velocity waveform and outlet pressure waveform (t_1 refers to the time at which systole occurs, $t_1/T = 0.2$; t_2 refers to waveform descending phase, $t_2/T = 0.27$; t_3 refers to the time at which diastole occurs, $t_3/T = 0.4$; $T = 1.2$ s is heart beat period).

nonlinear, large deformation dynamics were used. Before the final transient simulations were started, the mesh in a static case was refined until the result was independent of the mesh density. A mesh-independence study was performed before determining the optimal number of elements for the simulations. Four different mesh densities were explored before deciding final mesh. Maximum von Mises stress were compared between the four cases (mesh from coarse to fine). The last two cases had maximum von Mises stress difference $<0.1\%$, i.e., results are independent on mesh density. The total number of 8-node structure elements was 11,200. The luminal blood flow domain was meshed with 60,000 8-node fluid elements. The total number of elements at the FSI interfaces was 5400. In this simulation, a vari-

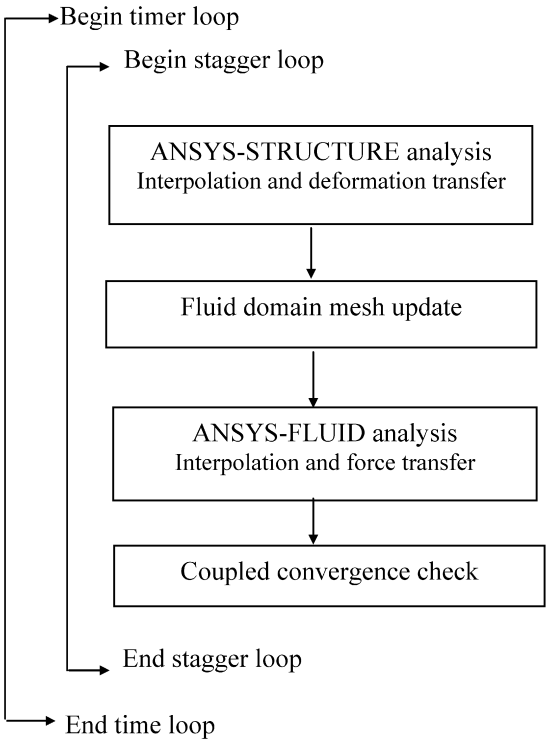

Fig. 2. Solution algorithm for fluid–structure interactions.

able time step was employed, where $\Delta t_{\min} = 0.005$ s with 60 total time steps per cycle. The convergence criterion for velocity, displacement and force at each time step was 0.05%. Between two successive cycles, the convergence criterion for pressure, velocity and displacement was 0.1%. Five cycles were required to achieve convergence for the transient analysis. Before the final simulations, mesh-independence of the results was successfully checked. Using a single processor of an IBM p690 workstation, the total CPU time was about 25 hours.

In addition to the numerical accuracy checks, the present computer simulation model was validated with matching comparisons between model predictions and experimental data sets [28,29] as discussed by Kleinstreuer et al. [30] as well as Li and Kleinstreuer [15,16] and Li [31].

3. Results and discussion

3.1. Hemodynamics

Considering three AAA configurations with different neck and iliac angles, of interest in this section are the transient 3-D blood flow patterns at distinct time levels during the cardiac cycle, i.e., at maximum inflow ($t/T = 0.2$; $Re = 1950$), maximum pressure ($t/T = 0.27$; $Re = 1000$), and maximum reverse flow ($t/T = 0.4$; $Re = -250$).

At $t/T = 0.2$, driven by the high inlet pressure, the blood flow accelerates to its maximum velocity (Fig. 3). It should be noted that only unit vectors were employed to indicate mid-plane blood flow structures. During peak systole, the mid-plane pressure and velocity in the AAA main-body appears to be nearly uniform. However, strong secondary flows occur as shown in the transverse slices, caused by the nonuniform blood vessel, wall movements, and transient flow conditions. Specifically, there are two symmetric vortex tubes inside slice B–B′. In slice C–C′, the blood flow forms two streams about to separate into the two iliac arteries, resulting in a near-zero velocity zone in front of the stagnant point. Somewhat remarkable is the fact that just before the bifurcation, the flow field is almost perfectly symmetric at that moment. Clearly, the secondary flow effect in slice C–C′ ($v_{\max} = 20$ cm/s) is much higher than in slice A–A′ ($v_{\max} = 10$ cm/s) or B–B′ ($v_{\max} = 6$ cm/s).

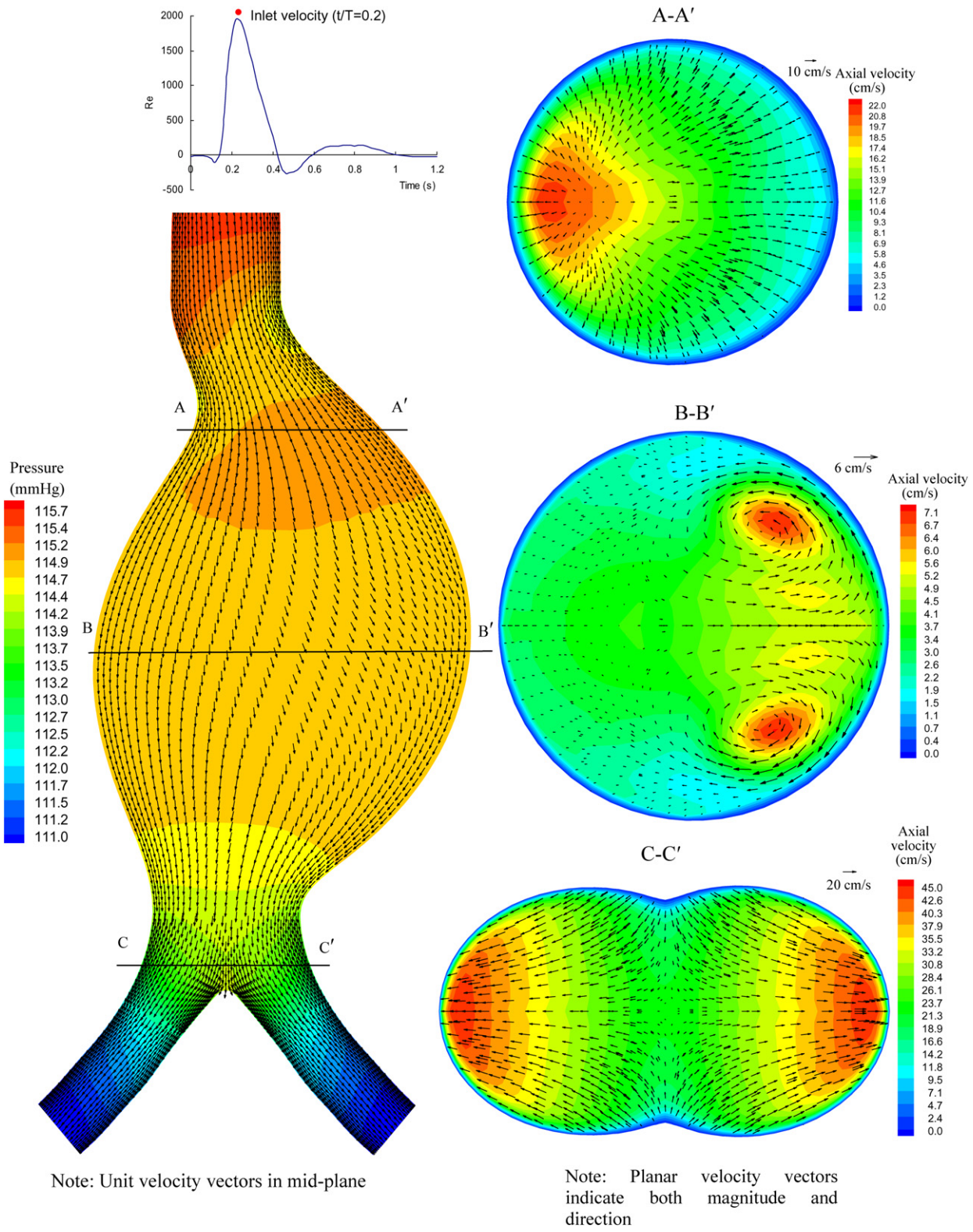

Fig. 3. Pressure and velocity distributions in AAA lumen ($t/T = 0.2$).

The blood flow is decelerating at $t/T = 0.27$ and the maximum pressure occurs near the iliac bifurcating point (Fig. 4). The main axial as well as the secondary flow fields have changed measurably in the proximal neck region. There appear now two vortices and flow separation points in mid-plane below the neck. Except slice A–A′, the flow pattern in axial and transverse direction remains similar as during peak flow (see Fig. 4 vs. Fig. 3)

When the dimensionless time t/T reaches 0.4, maximum backflow at $Re = -250$ occurs (Fig. 5). Two mid-plane vortices appear in the main section of the aneurysm, where one of them is now located near the center, associated with a low pressure area. Both the axial flow structure and secondary flow patterns are very different from the previous snapshots (cf. Figs. 4 and 5). The vortices in slice B–B′ have disappeared; but, two vortices occur before the bifurcation (see slice C–C′).

In summary, as a result of the given fluid flow conditions and wall material properties, the blood flow patterns are measurable influenced by the inlet/outlet waveforms, aneurysm geometry, and wall movement, i.e., fluid–structure interactions.

3.2. Effects of neck angle on flow patterns and Von Mises wall stress distributions

Lateral asymmetric AAAs. Although wall-stress values are almost the same for different neck angles from $\theta = 12°$ to $\theta = 45°$ at the three critical time levels in the lateral asymmetric AAA (Fig. 6, iliac bifurcation angle $\varphi = 90°$), the wall-stress distributions are very different for the three cases. Specifically, at $\theta = 12°$, the high wall-stress regions are towards the asymmetric bulge at all time levels, where the maximum stress occurs near the distal side toward the asymmetric bulge. However, as the neck angle increases, the proximal high-stress area shifts away from the asymmetric bulge, but still featuring $\sigma_{\max}$ at the same distal location. The reason is that a large neck angle causes strong surface curvatures in the AAA-neck, which leads to changing blood flow patterns near the proximal neck as well as a shift in elevated wall-stress region. This is in agreement with the findings by Elger et al. [32] and Sacks et al. [33], i.e., that an angulated neck could lead to elevated wall stresses. For example, at time level $t/T = 0.2$, there are no vortices if $\theta \leqslant 25°$. However, a small vortex occurs at the side away from the asymmetric bulge for $\theta = 45°$. In the decelerating phase $t/T = 0.27$, two reverse vortices are located near the proximal neck for both $\theta = 12°$ and $\theta = 25°$; but, for $\theta = 45°$ the flow field is very irregular, i.e., three different vortices were found while the main recirculation region includes a small sub-vortex. When $t/T = 0.4$, the flow direction is reversed, which causes three different vortices for $\theta = 12°$, two vortices for $\theta = 25°$ and one large vortex for $\theta = 45°$. Thus, the flow patterns are greatly affected by the neck angle.

Anterior-posterior asymmetric AAAs. Again, both flow patterns and wall-stress distributions in *anterior-posterior asymmetric AAAs* are significantly influenced by the neck angle (Fig. 7, iliac bifurcation angle $\varphi = 90°$). At $\theta = 12°$ and $\theta = 25°$, all high-stress regions are located at the anterior distal sides. However, it is of interest to note that the maximum wall-stress site moves to the posterior proximal area when $\theta = 45°$. Specifically, at time level $t/T = 0.2$, no vortex was found except for a small recirculation zone near the proximal neck when $\theta = 45°$. At $t/T = 0.27$, the decelerating flow produces two asymmetric vortices near the proximal neck for both $\theta = 12°$ and $\theta = 25°$. Clearly, at $\theta = 45°$, the large neck angle produces one large vortex near the posterior side and hence an elevated wall stress area.

When $t/T = 0.4$, the blood flow reverses, which results in very different flow patterns. Specifically, at $\theta = 12°$, there are two vortices rotating in the same direction in the center of the aneurysm and a small vortex zone near the posterior proximal neck. For $\theta = 25°$, one vortex region is located near the cavity center, another occurs near the anterior proximal neck. Interestingly, for $\theta = 45°$, the entire cavity is filled with a large vortex, as well as a small daughter vortex near the proximal neck.

It is noted that only the middle cross section has been graphed in this section. Actually, similar to Figs. 3–5, there are also "hidden" vortices at different levels of the horizontal cross sections, caused by secondary flows.

3.3. Effects of iliac bifurcation angle on flow patterns and Von Mises wall stress distributions

Lateral asymmetric AAA. As indicated in Fig. 8, flow patterns for the lateral asymmetric AAA change significantly at the three time levels, but hardly vary for the different bifurcation angles (neck angle $\theta = 25°$). During the accelerating phase ($t/T = 0.2$), no vortex exists in the AAA cavities, whereas two irregular vortices occur during the decelerating phase ($t/T = 0.27$, and 0.4). While the impact of a patient's iliac bifurcation angle on the flow field appears to be minor, its effect on the wall-stress distribution cannot be ignored. Specifically, small iliac angles may cause

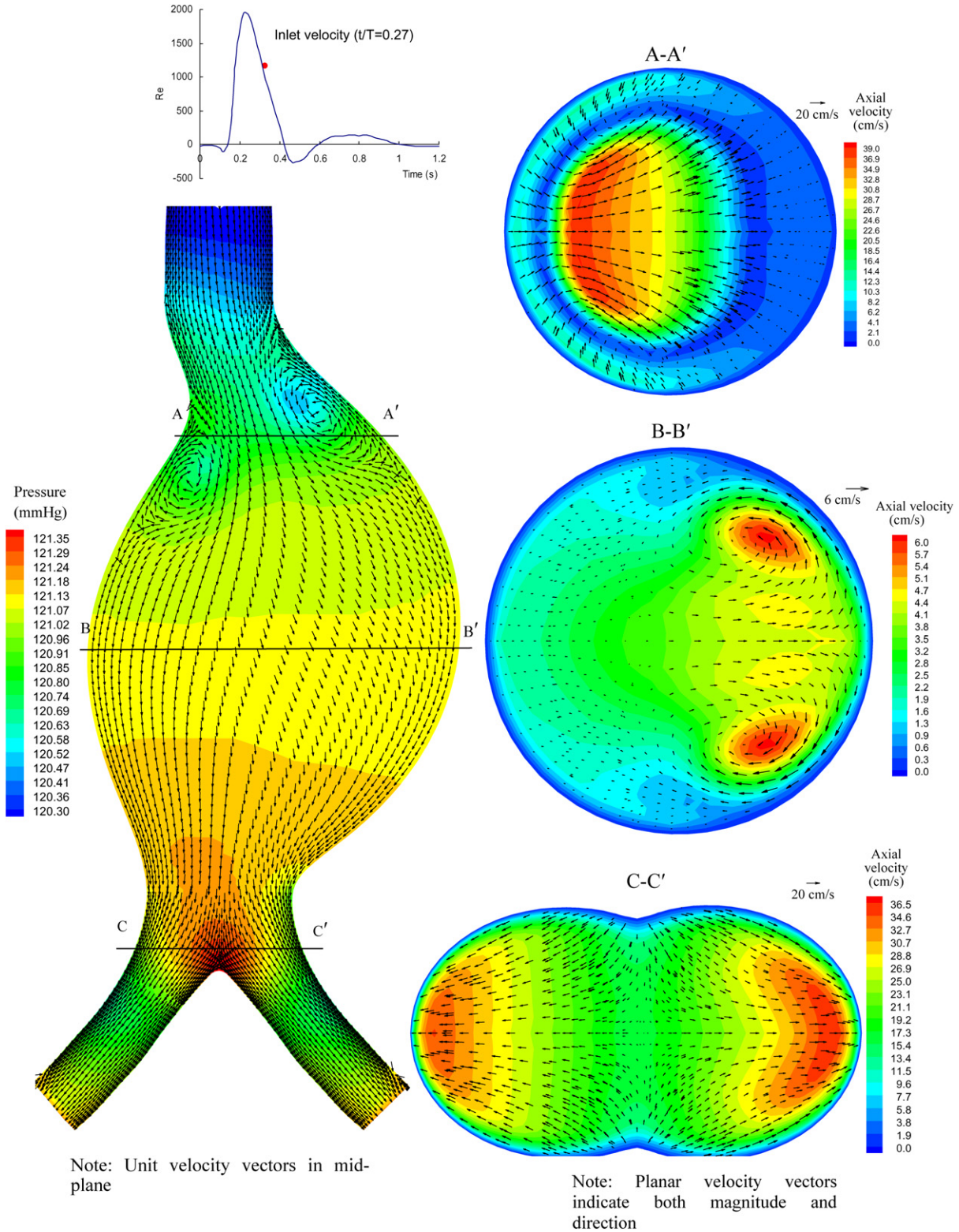

Fig. 4. Pressure and velocity distributions in AAA lumen ($t/T = 0.27$).

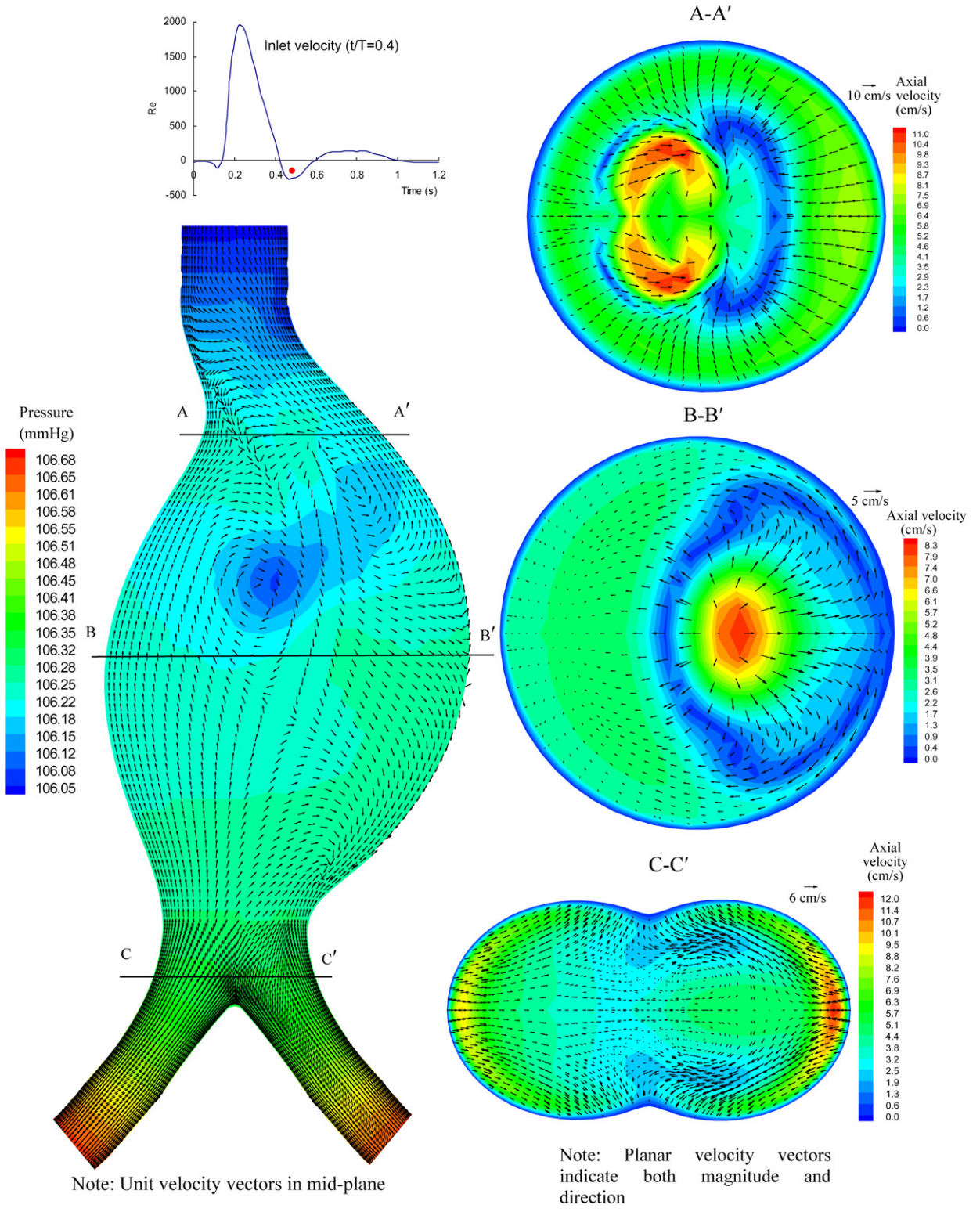

Fig. 5. Pressure and velocity distributions in AAA lumen ($t/T = 0.4$).

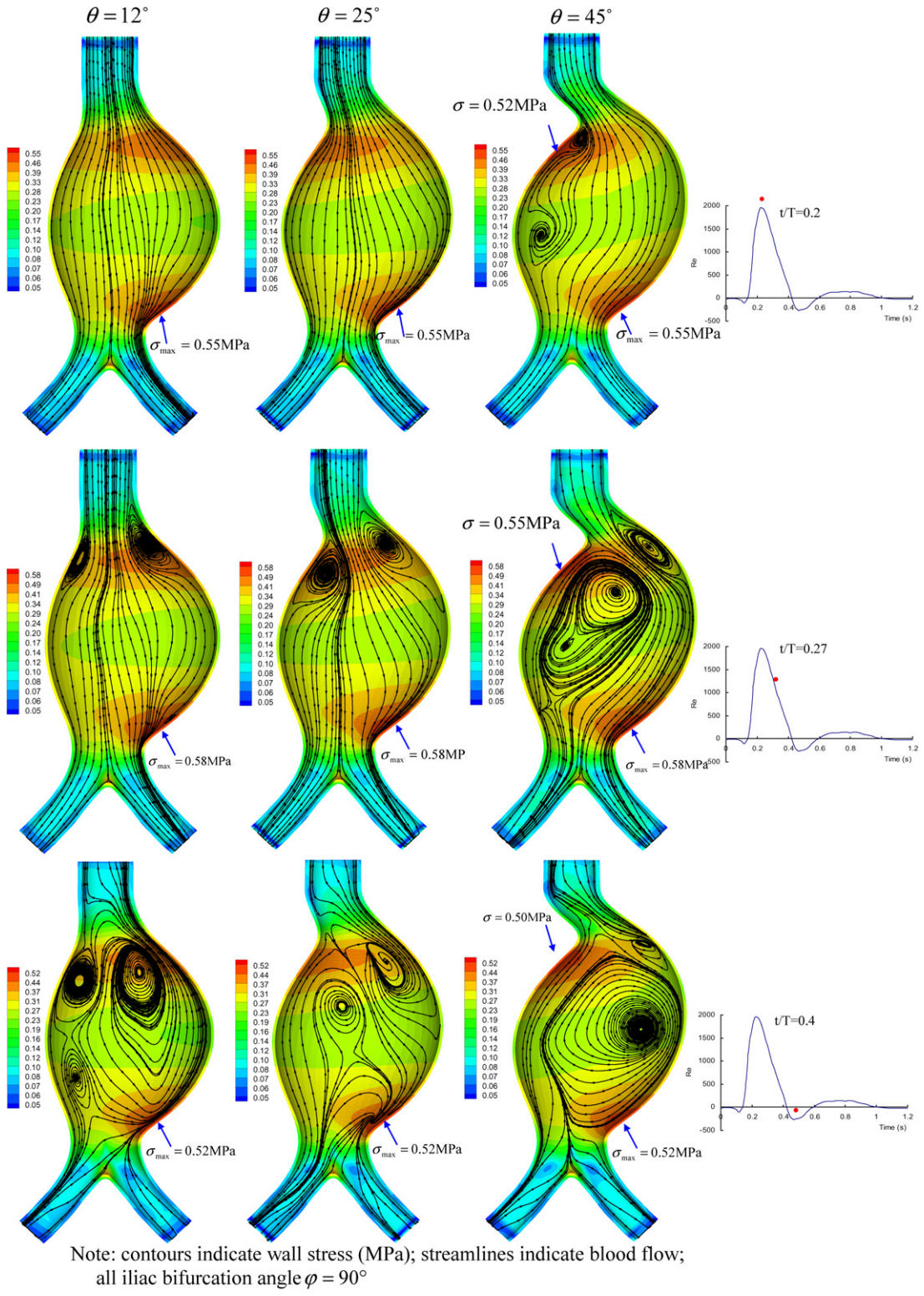

Fig. 6. Effects of neck angle on blood flow patterns and wall stress contours in lateral asymmetric AAA (iliac bifurcation angle $\varphi = 90°$).

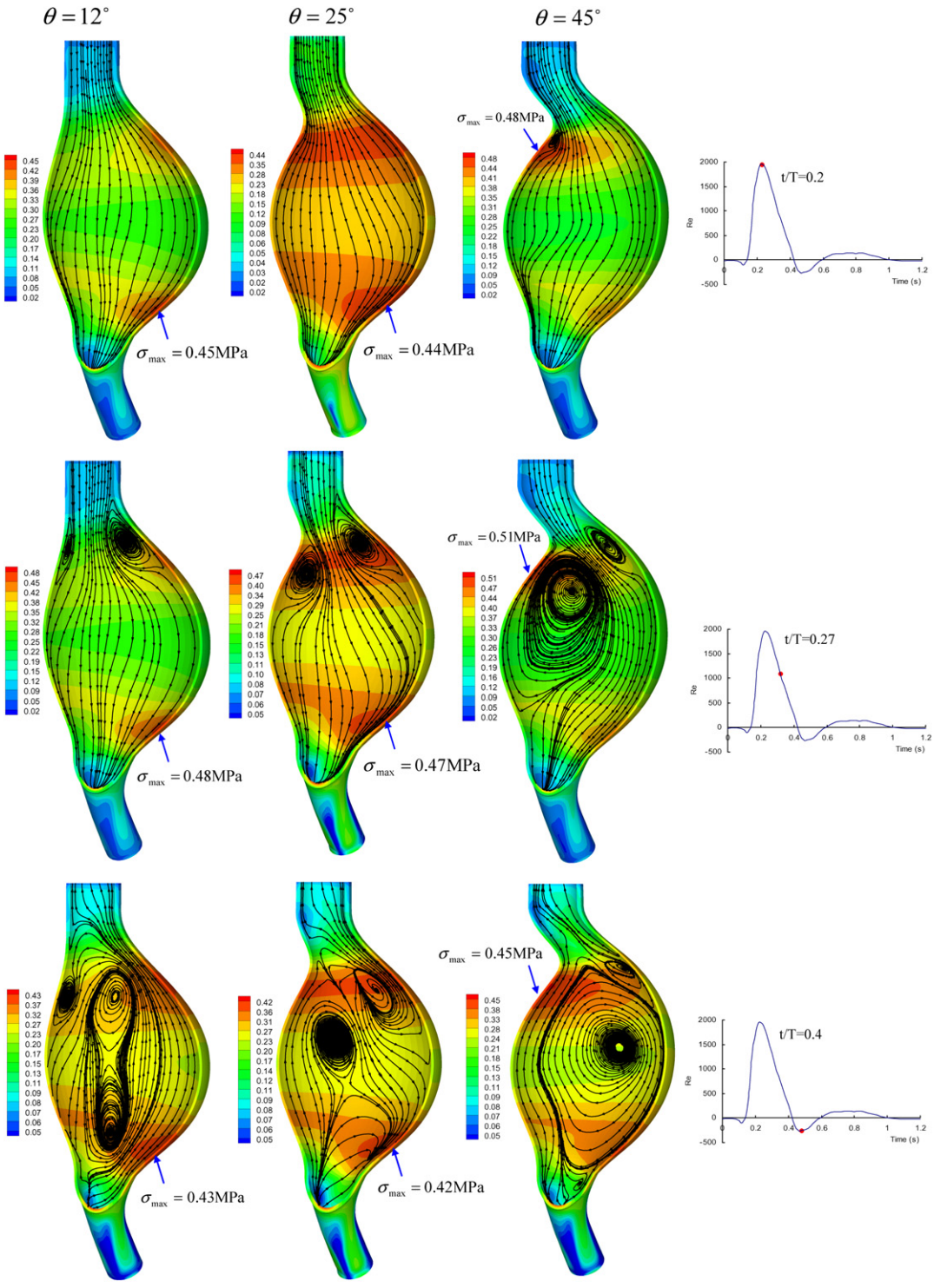

Fig. 7. Effects of neck angle on blood flow patterns and wall stress contours in anterior-posterior asymmetric AAA (iliac bifurcation angle $\varphi = 90°$).

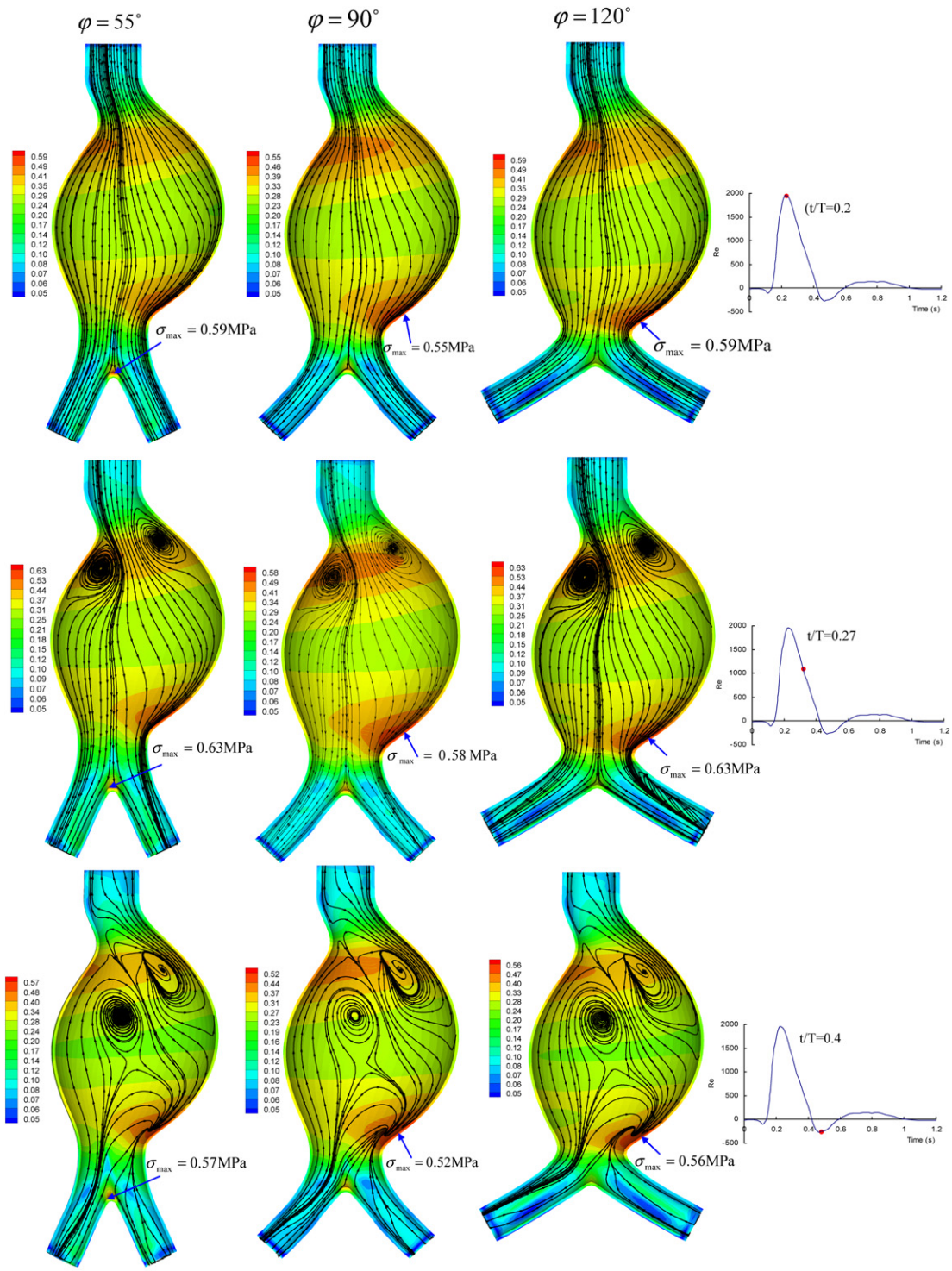

Fig. 8. Effects of iliac bifurcation angle on blood flow patterns and wall stress contours in lateral asymmetric AAA (neck angle $\theta = 25°$).

wall-stress concentrations in the junction area. For example, when $\varphi = 55°$, the maximum wall-stress located in the iliac bifurcation varies from 0.57 to 0.63 MPa for the three critical time levels. However, as the iliac angle increases, the maximum wall stress moves to the distal side towards the asymmetric bulge. Furthermore, once $\varphi \geqslant 90°$, the maximum wall stress increases with large iliac angles due to the strong curvatures near the distal side. For example, comparing $\varphi = 90°$ with$\varphi = 120°$, the maximum wall stress increases by about 8%.

Anterior-posterior asymmetric AAA. Similar to the lateral asymmetric AAA (Fig. 8), given the same geometry of the AAA main-body, the influence of the iliac bifurcation angle on flow patterns in the anterior-posterior asymmetric AAA is also insignificant. It is indicated that for any given time level, the flow patterns are very similar for the three different iliac angles (Fig. 9, neck angle $\theta = 25°$). But, it should be noted that for the small iliac angle $\varphi = 55°$, the maximum wall stress is located near the junction due to wall-stress concentrations. As the iliac angle φ increases, the maximum wall-stress moves from the divider wall area to the anterior distal side. The maximum wall stress also increases with large iliac angles, i.e., if $\varphi \geqslant 90°$. Comparing Fig. 9 to Fig. 8 implies that, even though the maximum AAA diameters are the same and the AAA main bodies are very similar, wall-stress magnitudes and distributions are very different between lateral asymmetric and anterior-posterior asymmetric AAAs. For any given time level, the wall stress in the lateral asymmetric AAA is much larger than that in the anterior-posterior asymmetric AAA. For example, at $t/T = 0.27$ and $\varphi = 120°$, the maximum wall stress in the anterior-posterior asymmetric AAA is 0.51 MPa, while the maximum wall-stress in the lateral asymmetric AAA is 0.63 MPa, i.e., an increase of 24%. It can be deduced that the rupture-risk of lateral asymmetric AAAs is higher than anterior-posterior asymmetric AAAs, if the maximum diameter is the same. The maximum wall stress-sites (see Fig. 9) are located near the anterior distal side for the anterior-posterior asymmetric AAA and near the distal side towards the asymmetric bulge for the lateral asymmetric AAA (see Fig. 8). Indeed, Golledge et al. [34] and Darling [35] found that 66–73% of AAA ruptures were located in the middle third close to the distal side.

3.4. Comparison of wall Von Mises stress distributions

Considering the critical time level $t/T = 0.27$, which coincides with the maximum pressure (see Fig. 1(b)), the comparison of wall stress distributions of three different configurations are illustrated in Fig. 10. For symmetric AAA, the maximum wall stress, $\sigma_{\max} = 0.44$ MPa, is located near the proximal neck. However, for the lateral asymmetric AAA, the maximum wall stress, $\sigma_{\max} = 0.58$ MPa, moves to distal side towards the asymmetric bulge. In the anterior-posterior asymmetric AAA, the maximum wall stress, $\sigma_{\max} = 0.47$ MPa, appears near the anterior distal side. In summary, for a given AAA main-body geometry, the wall stress in the lateral asymmetric AAA is much higher than in the anterior-posterior asymmetric AAA. The symmetric AAA has the lowest wall stress level and the assumption of symmetric AAA geometry may underestimate AAA-wall stress considerably.

3.5. Limitations

This study analyzed stress in relatively smooth, homogeneous and isotropic AAA. Clearly, patient-specific aneurysms exhibit wide variations in shape, size, mural thrombus, nonlinear material properties, and loading conditions. We assumed that the AAA wall is thinner at locations where the diameter is larger based on the measurement by Thubrikar et al. [19]. But if wall remodeling is considered, the thinner wall thickness is probably not at the maximum diameter. Another limitation is that we did not included wave propagation in the present flow study, which should be minor due to the very small inlet/outlet pressure differences in the AAAs under consideration. When local wall stresses are exceeding a given AAA-wall strength, AAA rupture will occur. However, AAA wall strength is spatially variable. For example, Thubrikar et al. [5] measured the wall yield stress and found that these values are not the same everywhere in the AAA wall, i.e., some regions of the AAA wall are weaker than others. Therefore, with a patient's yield stress field and wall-material properties unknown, any AAA-wall stress analysis has its limitations. The implementation of nonlinear wall properties in AAA models based on experimental data and CT-scans will be considered in future works. The third limitation is that an intra-luminal thrombus (ILT) was not considered in the model. Clinically, 75% of AAAs include thrombi. ITL is an accumulation of fibrin, blood cells, platelets, blood proteins and cellular debris adhering to the AAA inner wall. Some investigators think ILT may reduce the stress in the AAA wall. For example, Wang et al. [27] reported that the peak wall stress may be reduced from 6–38% if the ILT-AAA volume ratio ranges from 0.29–0.72. Thubrikar et al. [36] regarded ILT as a fibrous network adhering to

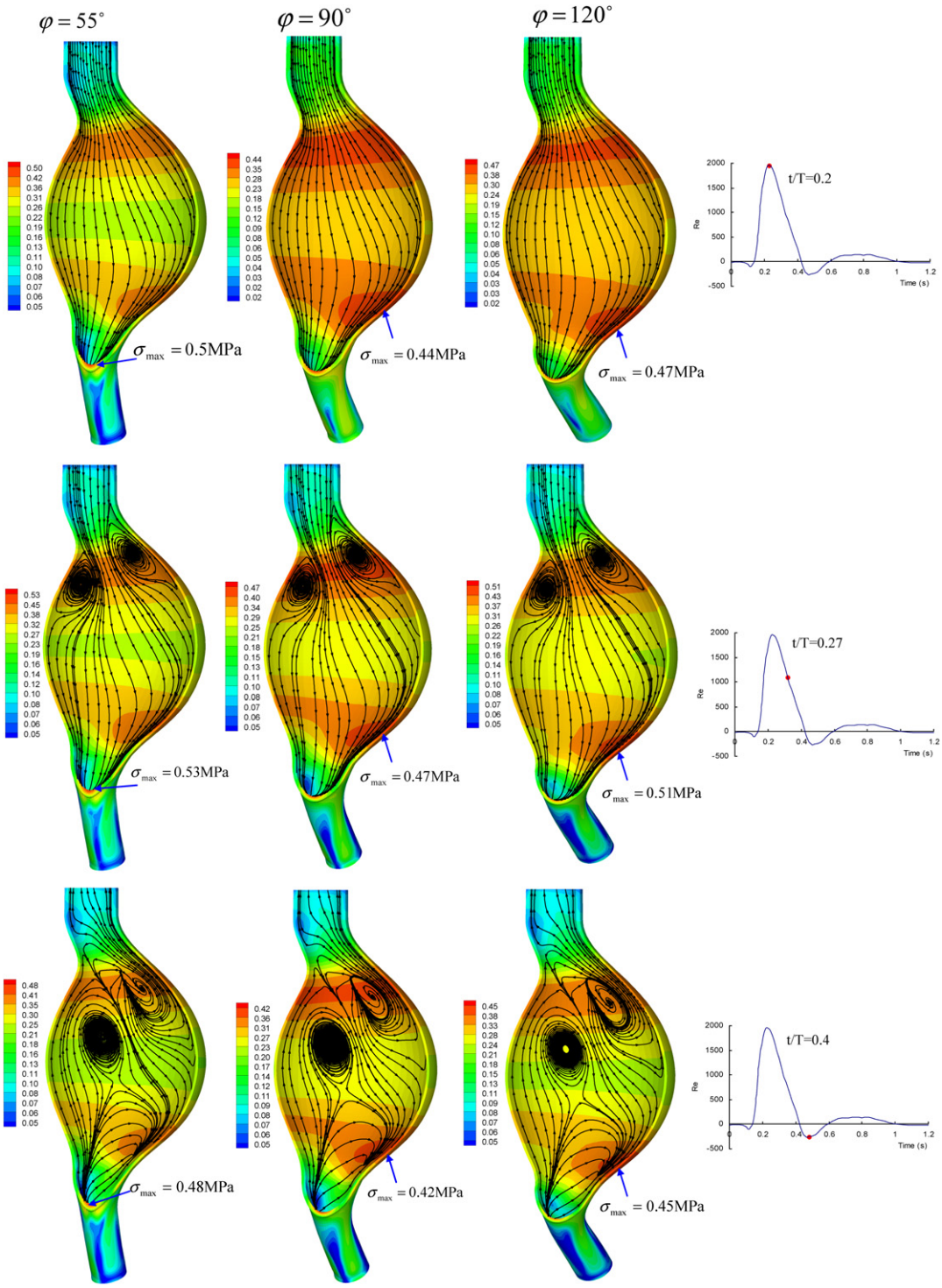

Fig. 9. Effects of iliac bifurcation angle on blood flow patterns and wall stress contours in anterior-posterior asymmetric AAA (neck angle $\theta = 25°$).

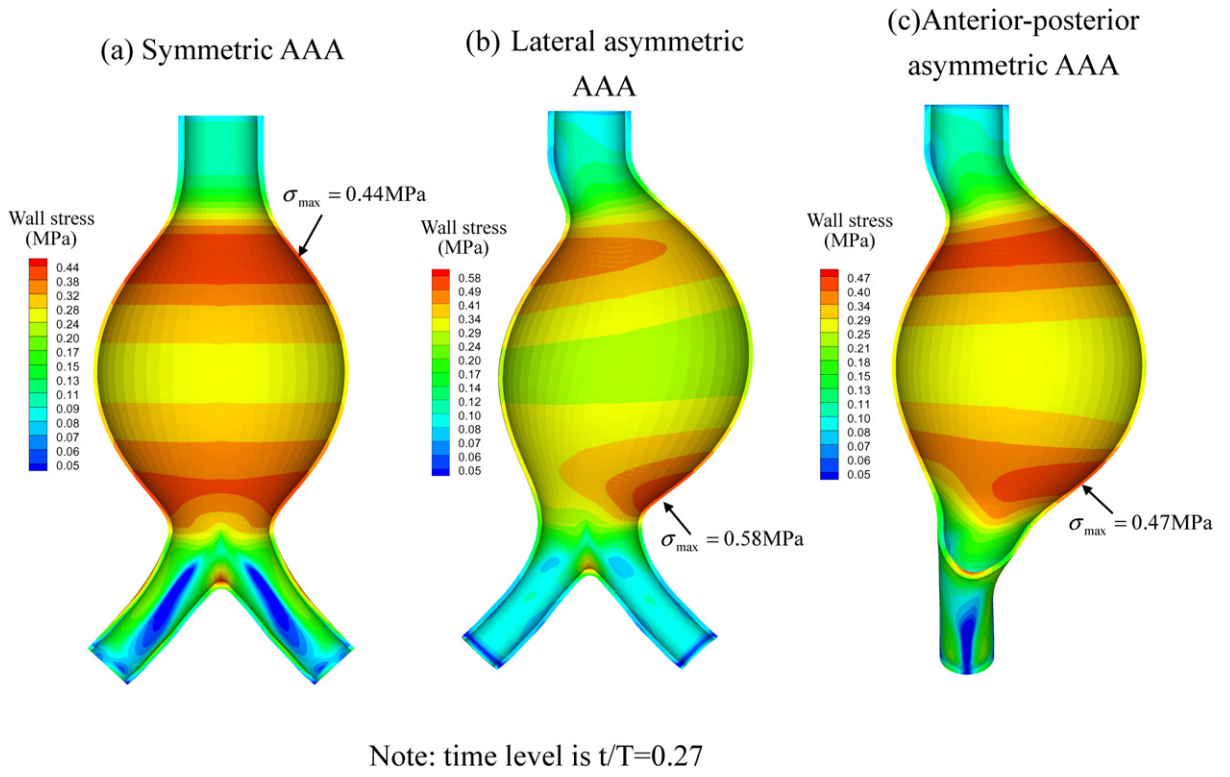

Fig. 10. Comparison of wall stress distributions for different AAAs ($t/T = 0.27$).

the aneurysm wall and may prevent the AAA from rupture. Vorp et al. [37] reported that an ILT could improve the compliance of the wall like a cushion, reduce mechanical stress. Mower et al. [20] simulated the ILT in an AAA and found that an ILT significantly reduced AAA wall-stress if the ILT became solid. Di Martino et al. [38] declared that a well-organized thrombus may reduce the effect of the pressure load on the AAA wall. In contrast, some researchers declared that ILTs could accelerate AAA rupture. For example, Wolf et al. [39] found that the larger the ILT volume in the AAA cavity, the higher is the possibility of rupture. Cappeller et al. [40] indicated that if the ILT/AAA volume ratio is more than 0.45, the rupture rate becomes very significant. Stenbaek et al. [41] investigated that patients with AAA ILT area increased by greater than 1.5 cm^2/year were prone to rupture. Interestingly, some researchers stated that there are no close relationship between ILT presence and AAA rupture. Schurink et al. [42] tested the blood pressure close to the inner wall of an AAA and found that the pressure is almost the same as that in the lumen. Our previous study indicated that the existence of a mural thrombus can help to reduce the AAA wall stress, if the decrease of wall yield stress caused by ILT is not considered [31]. However, Vorp et al. [43] stated that an ILT can decrease the ultimate AAA strength dramatically due to oxygen deficiency caused by an ILT. Therefore, if the degeneration of the wall strength is taken into account, the net effect of ILT on AAA wall rupture may vary. Without consideration of intra-luminal thrombus might affect wall stress magnitude and its distribution and hence rupture prediction. Therefore, more realistic AAA models with mural thrombus and AAA wall degeneration will be considered in our future work.

4. Conclusions

The following conclusions can be drawn from this fluid–structure interaction analysis.

(1) The neck angle impacts the blood flow fields substantially. A large neck angle may cause strong, irregular vortices in the AAA cavity. Also, the neck angle influences wall-stress distributions remarkably. A large neck angle, resulting in strong wall curvatures near the proximal neck, can produce aggravating blood flow patterns and elevated wall stresses.

(2) The iliac bifurcation angle affects blood flow patterns insignificantly but plays an important role in wall-stress concentrations.
(3) The maximum wall stress of lateral asymmetric AAAs is higher than for the anterior-posterior asymmetric types. The highest wall stress is located near the anterior distal side for the anterior-posterior asymmetric AAA and the distal side towards the asymmetric bulge in the lateral asymmetric AAA.
(4) The assumption of *symmetric* AAA geometry may underestimate AAA-wall stress and hence rupture-risk assessment considerably. Thus, symmetric AAA models cannot accurately represent AAA-wall stresses and flow fields.
(5) Fluid–structure interaction simulations may provide physical insight into the hemodynamics and biomechanics of AAAs and hence a better understanding of blood flow fields, maximum wall-stress and their locations, and ultimately AAA-rupture risk.

Acknowledgements

The authors acknowledge the use of ANSYS ALE FSI from Ansys Inc. (Canonsburg, PA) as well as the AAA geometries and clinical insight provided by Mark Farber, endovascular surgeon at UNC-CH, School of Medicine.

References

[1] M.F. Fillinger, M.L. Raghavan, P. Marra, L. Cronenwett, E. Kennedy, In vivo analysis of mechanical wall stress and abdominal aortic aneurysm rupture risk, Journal of Vascular Surgery 36 (2000) 589–596.
[2] M.F. Fillinger, P.S. Marra, M.L. Raghavan, E.F. Kennedy, Prediction of rupture in abdominal aortic aneurysm during observation: Wall stress versus diameter, Journal of Vascular Surgery 37 (2003) 724–732.
[3] H. Yamada, E. Tanaka, S. Murakami, Mechanical evaluation of growth and rupture of aneurysm in abdominal aorta, JSME International Journal Series A – Mechanics and Material Engineering 37 (1994) 181–187.
[4] M. Raghavan, D. Vorp, M. Federle, M. Makaroun, M. Webster, Wall stress distribution on three-dimensionally reconstructed models of human abdominal aortic aneurysm, Journal of Vascular Surgery 31 (2000) 760–769.
[5] M. Thubrikar, M. Labrosse, F. Robicsek, J. Al-Soudi, Mechanical properties of abdominal aortic ansuerysm wall, Journal of Medical Engineering & Technology 25 (2000) 133–142.
[6] D.A. Vorp, M. Raghavan, M. Webster, Mechanical wall stress in abdominal aortic aneurysm: influence of diameter and asymmetry, Journal of Vascular Surgery 27 (1998) 632–639.
[7] E.A. Finol, K. Keyhani, C.H. Amon, The effect of asymmetry in abdominal aortic aneurysms under physiologically realistic pulsatile flow conditions, Journal of Biomechanical Engineering – Transactions of the ASME 125 (2003) 207–217.
[8] E.A. Finol, E.S. Di Martino, D.A. Vorp, C.H Amon, Biomechanics of patient specific abdominal aortic aneurysms: Computational analysis of fluid flow, in: Proceedings of the 28th Annual IEEE Northeast Bioengineering Conference, Philadelphia, PA, April 20–21, 2002, pp. 191–192.
[9] R. Peattie, C. Asbury, E. Bluth, J. Ruberti, Steady flow in models of abdominal aortic aneurysms (Part I), Journal of Ultrasound Medicine 15 (1996) 679–688.
[10] T. Yip, S. Yu, Cyclic transition to turbulence in rigid abdominal aortic aneurysm models, Fluid Dynamics Research 29 (2001) 81–113.
[11] S. Yu, Steady and pulsatile flow studies on abdominal aortic aneurysm models using Particle Image Velocimetry, Heat and Fluid Flow 21 (2000) 74–83.
[12] E.S. Di Martino, G. Guadagni, A. Fumero, G. Ballerini, R. Spirito, P. Biglioli, A. Redaelli, Fluid–structure interaction within realistic three-dimensional models of the aneurysmatic aorta as a guidance to assess the risk of rupture of the aneurysm, Medical Engineering and Physics 23 (2001) 647–655.
[13] E.S. Di Martino, G. Guadagni, A. Fumero, R. Spirito, A. Redaelli, A computational study of the fluid–structure interaction within a realistic aneurysmatic vessel model obtained from CT scans image processing, in: J. Middleton, M. Jones, N. Shrive, G. Pande (Eds.), Computer Methods in Biomechanics and Biomedical Engineering, third ed., Gordon and Breach Science Publishers, Newark, NJ, 2002, pp. 719–724.
[14] E.A. Finol, E.S. Di Martino, D.A. Vorp, C.H. Amon, Fluid–structure interaction and structural analyses of an aneurysm model, in: Proceedings of the ASME 2003 Summer Bioengineering Conference, Key Biscayne, FL, June 25–29, 2003, pp. 75–76.
[15] Z. Li, C. Kleinstreuer, Fluid–structure interaction effects on sac-blood pressure and wall stress in a stented aneurysm, Journal of Biomechanical Engineering (ASME) 127 (2005) 662–671.
[16] Z. Li, C. Kleinstreuer, Blood flow and structure interactions in a stented abdominal aortic aneurysm model, Medical Engineering & Physics 27 (2005) 369–382.
[17] D. Quemada, Rheology of concentrated disperse system III, General features of proposed non-Newtonian model. Comparison with experimental data, Rheological Acta 17 (1978) 643–653.
[18] J.R. Buchanan, C. Kleinstreuer, J.K. Comer, Rheological effects on pulsatile hemodynamics in a stenosed tube, Computers & Fluids 29 (2000) 695–724.
[19] M. Thubrikar, J. Al-Soudi, F. Robicsek, Wall stress studies of abdominal aortic aneurysm in a clinical model, Annals of Vascular Surgery 3 (2001) 355–366.

[20] W.R. Mower, W.J. Quinones, S.S. Gambhir, Effect of intraluminal thrombus on abdominal aortic aneurysm wall stress, Journal of Vascular Surgery 26 (1997) 602–608.
[21] F. Inzoli, F. Boschetti, M. Zzppa, T. Longo, R. Fumero, Biomechanical factors in abdominal aortic-aneurysm rupture, European Journal of Vascular Surgery 7 (1993) 667–674.
[22] J. Hua, R. Mower, Simple geometric characteristics fail to reliable predict abdominal aortic aneurysm wall stress, Journal of Vascular Surgery 34 (2001) 308–315.
[23] M.L. Raghavan, D.A. Vorp, Toward a biomechanical tool to evaluate rupture potential of abdominal aortic aneurysm: identification of a finite strain constitutive model and evaluation of its applicability, Journal of Biomechanics 33 (2000) 475–482.
[24] C. Taylor, T. Hughes, C. Zarins, Finite element modeling of three-dimensional pulsatile flow in the abdominal aorta: Relevance to atherosclerosis, Annals of Biomedical Engineering 26 (1998) 975–987.
[25] B. Wolters, M. Rutten, G. Schurink, U. Kose, J. de Hart, F. van de Vosse, A patient-specific computational model of fluid–structure interaction in abdominal aortic aneurysms, Medical Engineering & Physics 27 (2005) 871–883.
[26] O. Meter, Numerical simulation and experimental validation of blood flow in arteries with structured-tree outflow conditions, Annals of Biomedical Engineering 28 (2000) 1281–1299.
[27] D. Wang, M. Makaroun, M. Webster, D.A. Vorp, Effect of intraluminal thrombus on wall stress in patient specific model of abdominal aortic aneurysm, Journal of Vascular Surgery 3 (2002) 598–604.
[28] M. Gawenda, P. Knez, S. Winter, G. Jaschke, G. Wassmer, T. Schmitz-Rixen, J. Brunkwall, Endotension is influenced by wall compliance in a latex aneurysm model, European Journal of Vascular and Endovascular Surgery 27 (2004) 45–50.
[29] H.S. Flora, B. Talei-Faz, L. Ansdell, E.J. Chaloner, A. Sweeny, A. Grass, M. Adiseshiah, Aneurysm wall stress and tendency to rupture are features of physical wall properties: An experimental study, Journal of Endovascular Therapy 9 (2002) 665–675.
[30] C. Kleinstreuer, Z. Li, M.A. Farber, Fluid–structure interaction analyses of stented abdominal aortic aneurysm, Annual Rewiews of Biomedical Engineering 9 (2007) 5.1–5.36.
[31] Z. Li, Computational analysis and simulations of fluid–structure interactions for stented abdominal aortic aneurysms, PhD dissertation, North Carolina State University, 2005.
[32] D.F. Elger, D.M. Blackketter, R.S. Budwig, K.H. Johansen, The influence of shape on the stresses in model abdominal aortic aneurysms, Journal of Biomechanical Engineering (ASME) 118 (1996) 326–332.
[33] M.S. Sacks, D.A. Vorp, M.L. Raghavan, M.P. Federle, M.W. Webster, In vivo three-dimensional surface geometry of abdominal aortic aneurysms, Annals of Biomechanical Engineering 27 (1999) 469–479.
[34] J. Golledge, J. Abrokwah, K.N. Shenoy, R.H. Armour, Morphology of ruptured abdominal arotic aneurysms, European Vascular and Endovascular Surgery 18 (1999) 96–104.
[35] R.C. Darling, Ruptured arteriosclerotic abdominal aortic aneurysms, American Journal of Surgery 119 (1970) 397–401.
[36] M. Thubrikar, F. Robicsek, M. Labrosee, V. Chervenkoff, Effect of thrombus on abdominal aortic aneurysm wall dilation and stress, Journal of Cardiovascular Surgery 44 (2003) 67–77.
[37] D.A. Vorp, W.A. Mandarino, M.W. Webster, J. Gorcsan, Potential influence of intraluminal thrombus on abdominal aortic aneurysm as assessed by a new non-invasive method, Cardiovascular Surgery 4 (1996) 732–739.
[38] E. Di Martino, S. Mantero, F. Inzoli, G. Melissano, D. Astore, R. Chiesa, R. Fumero, Biomechanics of abdominal aortic aneurysm in the presence of endoluminal thrombus: experimental characterization and structural static computational analysis, European Vascular and Endovascular Surgery 15 (1998) 290–299.
[39] Y.G. Wolf, W.S. Thomas, F.J. Brennan, W.G. Goff, M.J. Sise, E.F. Bernstein, Computed tomography scanning findings associated with rapid expansion of abdominal aortic aneurysms, Journal of Vascular Surgery 20 (1994) 529–538.
[40] W.A. Cappeller, H. Engelmann, S. Blechschmidt, M. Wild, L. Lauterjung, Possible objectification of a critical maximum diameter for elective surgery in abdominal aortic aneurysms based on one- and three-dimensional ratios, Journal of Cardiovascular Surgery 38 (1997) 623–628.
[41] J. Stenbaek, B. Kalin, J. Swedenborg, Growth rate of thrombus may be a better predictor of rupture than diameter in patients with abdominal aortic aneurysm, European Vascular and Endovascular Surgery 20 (2000) 466–469.
[42] G. Schurink, N. Aarts, M. Malina, J.V. Bockel, Pulsatile wall motion and blood pressure in aneurysms with open and thrombosed endoleaks-comparison of a wall track system and M-mode ultrasound scanning: An in vitro and animal study, Journal of Vascular Surgery 32 (2000) 759–766.
[43] D.A. Vorp, P.C. Lee, D.H. Wang, M.S. Makaroun, E.M. Nemoto, M.W. Ogawa, S. Webster, Association of intraluminal thrombus in abdominal aortic aneurysm with local hypoxia and wall weakening, Journal of Vascular Surgery 34 (2001) 291–299.